# Collective Dipolar Interactions in Self-Assembled Magnetic Binary Nanocrystal Superlattice Membranes

**ARTICLE** *in* NANO LETTERS · NOVEMBER 2010

Impact Factor: 13.59 · DOI: 10.1021/nl103568q · Source: PubMed



**7 AUTHORS**, INCLUDING:

Angang Dong
Fudan University
**37** PUBLICATIONS **1,669** CITATIONS
SEE PROFILE

Xingchen Ye
University of California, Berkeley
**57** PUBLICATIONS **2,753** CITATIONS
SEE PROFILE

Christopher B Murray
University of Pennsylvania
**259** PUBLICATIONS **27,426** CITATIONS
SEE PROFILE

NANO LETTERS

pubs.acs.org/NanoLett

# Collective Dipolar Interactions in Self-Assembled Magnetic Binary Nanocrystal Superlattice Membranes

Jun Chen,[†,⊥] Angang Dong,[*,†,∥,⊥] Jing Cai,[§] Xingchen Ye,[†] Yijin Kang,[†] James M. Kikkawa,[§] and Christopher B. Murray[*,†,‡]

[†]Department of Materials Science and Engineering, [‡]Department of Chemistry, and [§]Department of Physics and Astronomy, University of Pennsylvania, Philadelphia, Pennsylvania 19104, United States and [∥]The Molecular Foundry, Lawrence Berkeley National Laboratory, Berkeley, California 94720, United States

**ABSTRACT** Co-assembly of two types of nanocrystals (NCs) into binary NC superlattices (BNSLs) provides a solution-based, inexpensive way to create novel metamaterials with rationally designed properties. The fundamental challenge is to probe and understand the nature and extent of complex interparticle interactions present in BNSLs, which can lead to collective properties that differ from their dispersed constituents or phase-separated counterparts. Here, we report the growth and magnetic characterization of large-area (~1 $cm^2$) BNSL membranes self-assembled from distinct magnetic NCs at the liquid−air interface. The resulting BNSL membranes exhibit a single-phase-like magnetization alignment process, which is not observed in the phase-separated NC mixtures having the same stoichiometry. This single-phase-like magnetic behavior is attributed to the collective interparticle dipolar interactions between two NC components in BNSLs, corroborated by calculation of the random dipolar fields as well as Monte Carlo simulation. The collective magnetic properties are demonstrated in magnetic BNSL membranes having different structures (stoichiometry) and different NC combinations.

**KEYWORDS** Binary nanocrystal superlattices, BNSLs, dipolar interactions, collective properties, Monte Carlo simulation

Long-range-ordered arrays or superlattices self-assembled from monodisperse nanocrystals (NCs) are attracting great attention because of their potential applications in electronic, optoelectronic, and magnetic devices.[1−7] The device performance is dictated by the properties of individual NCs as well as their mutual interactions. Recent advances in colloidal self-assembly enable the construction of binary NC superlattices (BNSLs),[8−16] in which two types of NCs (distinct in compositions and/or sizes) are coassembled into ordered arrays with precisely controlled NC packing symmetry, stoichiometry, and interparticle spacing. Compared to the single-component NC superlattices, interparticle interactions present in BNSLs are more complicated with collective properties that are not simply the sum of individual NC properties.[17,18] This opens up vast opportunities to create new materials with rationally designed properties by tuning NC combinations and superlattice structures, provided that we can better understand the nature and extent of interparticle interactions. In this regard, binary superlattices consisting of two types of magnetic NCs serve, both theoretically and experimentally, as an ideal system to probe collective magnetic behaviors of multicomponent NC systems. The primary interparticle interactions in magnetic NC assemblies may manifest through exchange[19−22] or dipole−dipole interactions,[23−28] depending on the interparticle spacing.

Here we report for the first time experimental evidence of collective interparticle dipolar interactions present in BNSLs self-assembled from distinct superparamagnetic NCs. This collective magnetic behavior is manifested in a single-phase-like magnetization alignment process, which is not observed in the phase-separated NC mixtures having the identical stoichiometry. The recently developed liquid−air interfacial assembly approach enables the rapid growth of large-area (~1 $cm^2$), high-quality BNSL membranes that can be readily transferred to arbitrary substrates,[10] allowing us to explore complicated interparticle interactions present in multicomponent NC superlattices. We choose BNSLs consisting of two different-sized $Fe_3O_4$ NCs as a model system to demonstrate collective magnetic properties, as dipolar interparticle interactions of single-component $Fe_3O_4$ NCs have been widely studied in ferrofluids,[29] dispersions[30] and close-packed arrays,[31,32] due to the low magnetocrystalline anisotropy energy of $Fe_3O_4$.[33]

Monodisperse $Fe_3O_4$ NCs with controllable sizes are synthesized according to literature procedures and are dissolved in hexane to form stable colloidal dispersions.[34] To grow BNSL membranes, a drop of hexane solution containing two different-sized $Fe_3O_4$ NCs with selected NC number ratios is dropcast onto the surface of diethylene glycol (DEG) in a Teflon well.[10] The growth of BNSLs is initiated by solvent

* To whom correspondence should be addressed. E-mail: (A.D.) adong@lbl.gov; (C.B.M.) cbmurray@sas.upenn.edu.

[⊥] These authors contributed equally to this work.

**Received for review:** 10/12/2010
**Published on Web:** 11/11/2010





DOI: 10.1021/nl103568q | *Nano Lett.* **2010,** *10,* 5103–5108

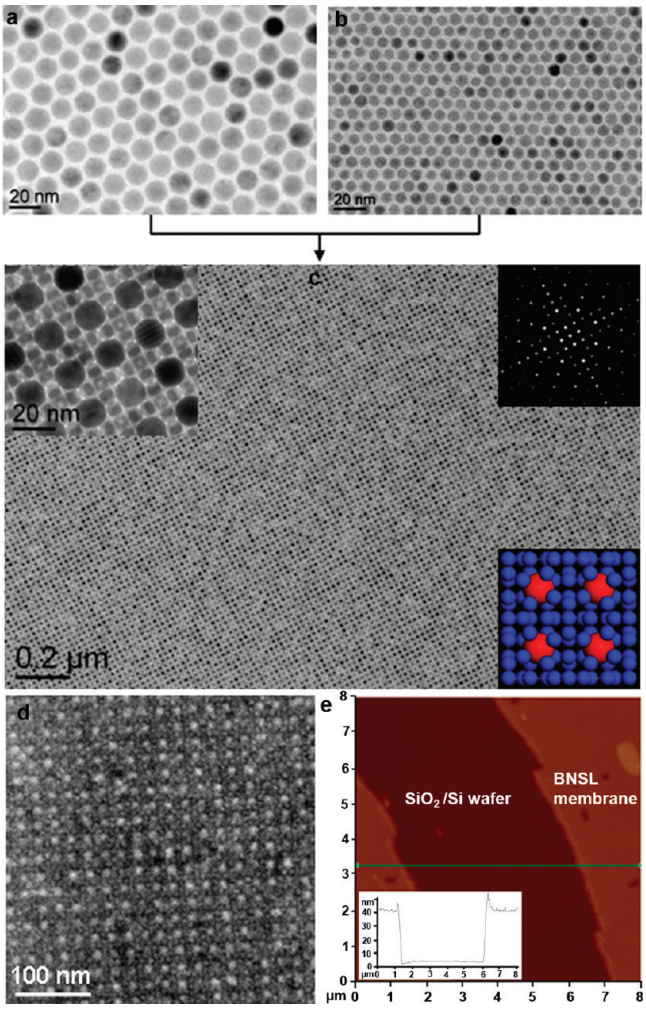


**FIGURE 1. TEM images of (a) 14.3 nm $Fe_3O_4$ NCs and (b) 7.2 nm $Fe_3O_4$ NCs used for the self-assembly of BNSL membranes. (c) TEM image, magnified view (upper left inset), small-angle electron diffraction pattern (upper right inset), and structural model (lower right inset) of a typical ico-$AB_{13}$-type BNSL membrane self-assembled from 14.3 and 7.2 nm $Fe_3O_4$ NCs along the (001) lattice projection. (d) SEM image of an ico-$AB_{13}$-type BNSL membrane along the (001) lattice projection. (e) AFM height image of an ico-$AB_{13}$-type BNSL membrane transferred to a $SiO_2$−Si wafer. Inset shows the height profile analysis as indicated in the AFM image, showing the membrane thickness is ~40 nm.**

evaporation at room temperature, yielding a continuous solid membrane supported on the DEG surface when the evaporation of hexane is complete. The resulting BNSL membranes are transferred to carbon-coated transmission electron microscopy (TEM) grids or $SiO_2$/Si wafers for structural (TEM, scanning electron microscopy (SEM), and atomic force microscopy (AFM)) and magnetic property characterization.

TEM establishes the high monodispersity of two $Fe_3O_4$ NC components used for the self-assembly of BNSL membranes (Figure 1a,b and Supporting Information Figure S1). The average sizes determined from statistical analysis are 14.3 nm ± 0.6 nm and 7.2 nm ± 0.4 nm, respectively (Supporting Information Figure S2). Drying-mediated co-crystallization of these two different sized $Fe_3O_4$ NCs results in large-area BNSL membranes, the structure of which is tunable by varying the number ratio between two NC components. Figure 1c shows the TEM image of a typical ico-$AB_{13}$-type BNSL membrane along the (001) lattice projection and its long-range-ordered superlattice structure is confirmed by small-angle electron diffraction (Figure 1c, upper right inset). In the cubic ico-$AB_{13}$ superlattice structure, each larger A-site $Fe_3O_4$ NC is surrounded by eight icosahedra, while each icosahedron consists of 13 smaller B-site $Fe_3O_4$ NCs,[16] as schematically illustrated in Figure 1c (lower right inset). The membrane is comprised of binary superlattice domains having different growth directions and/or different orientations, as evidenced by grain boundaries between neighboring domains (Supporting Information Figure S3). It is noteworthy that the (001) lattice projection is predominant in ico-$AB_{13}$-type BNSL membranes, although the (011) projection is also observed in some cases (Supporting Information Figure S4). SEM reveals the membrane is of uniform thickness, consisting of BNSL domains with average lateral sizes of 1−2 $\mu$m (Figure 1d and Supporting Information Figure S5). The typical membrane thickness determined from AFM is ~40 nm (Figure 1e), roughly corresponding to one unit cell, which consists of two layers of larger NCs and two layers of icosahedra composed of smaller NCs. The propagating sharp crack provides further evidence of the long-range-ordered superlattice structure of the BNSL membrane.[10]

In-plane dc magnetization measurements of BNSL membranes are performed on a commercial superconducting quantum interference device (SQUID) magnetometer. Figure 2a shows the zero-field-cooled (ZFC) and field-cooled (FC) magnetization curves for two different-sized $Fe_3O_4$ NCs and the resulting ico-$AB_{13}$-type BNSL membrane, respectively, which are acquired in the presence of an applied magnetic field of 100 Oe. The blocking temperatures ($T_b$) of 14.3 and 7.2 nm $Fe_3O_4$ NCs are 209 and 68 K, respectively, determined from the maximum in the corresponding ZFC curves. The higher $T_b$ of 14.3 nm $Fe_3O_4$ NCs is attributed to the higher magnetocrystalline anisotropy energy barrier arising from the larger NC volume.[34] Notably, the ZFC curve of the BNSL membrane only shows one maximum at 158 K (Figure 2a, blue curve), which is located between the $T_b$ of two NC single components. This single-phase-like magnetization alignment process suggests a collective magnetic behavior, presumably arising from interparticle interactions between two NC components in BNSLs.

To further investigate interparticle interactions present in BNSLs, we qualitatively compare the ZFC/FC curves of BNSLs with those of phase-separated NC mixtures having the same $AB_{13}$ stoichiometry (Figure 2b). In an ensemble of two types of NCs (A and B) without A-B interparticle interactions, the total magnetization ($M_{total}(T)$) at a specific temperature ($T$)



DOI: 10.1021/nl103568q | *Nano Lett.* **2010,** *10,* 5103–5108

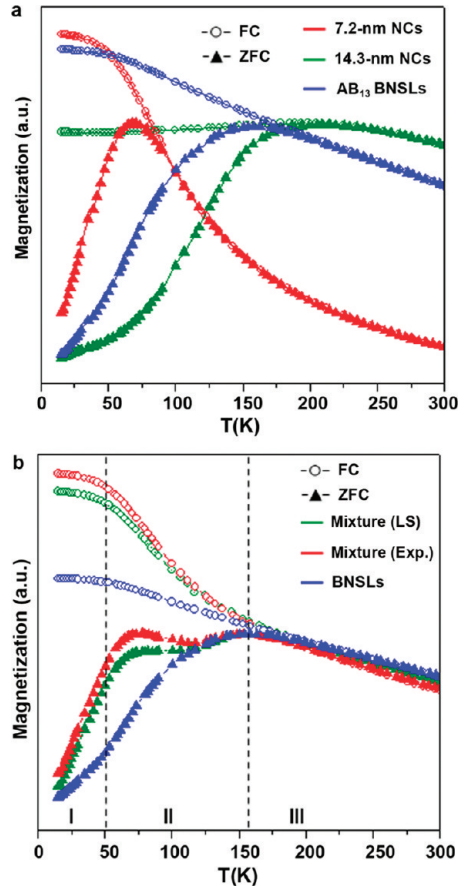


**FIGURE 2. (a) ZFC/FC curves for 14.3 nm $Fe_3O_4$ NCs (olive), 7.2 nm $Fe_3O_4$ NCs (red), and the resulting ico-$AB_{13}$-type BNSL membrane self-assembled from these two NC components (blue). (b) Linear superposition (LS) ZFC/FC curves (olive) and experimental ZFC/FC curves (red) of the phase-separated mixtures consisting of 14.3 and 7.2 nm $Fe_3O_4$ NCs with the NC number ratio of 1:13, and ZFC/FC curves (blue) of the ico-$AB_{13}$-type BNSL membrane self-assembled from 14.3 and 7.2 nm $Fe_3O_4$ NCs.**

would simply be a weighted sum of the magnetization of two NC components, $M_A(T)$ and $M_B(T)$

$$M_{total}(T) = m_A M_A(T) + m_B M_B(T) \quad (1)$$

where $m_A$ and $m_B$ are the weight percentages of A and B, respectively.[35] In other words, the ZFC/FC curves of a phase-separated mixture should be the linear superposition (LS) of the ZFC/FC curves corresponding to each NC component. We separately acquire the ZFC/FC curves for two different-sized $Fe_3O_4$ NCs with the NC number ratio of 1:13, which are then combined mathematically to form the superposition curves (Figure 2b, olive curves). The LS ZFC/FC curves are also created experimentally (Figure 2b, red curves) by measuring the magnetization of a phase-separated NC mixture with the stoichiometry of 1:13, which is prepared by separately depositing the two different sized $Fe_3O_4$ NCs onto the two sides of the same $SiO_2$/Si wafer (~500 $\mu$m in thickness). In contrast to the ZFC curve of the BNSL membrane (Figure 2b, blue curve), the ZFC curves for the phase-separated NC mixtures obtained in both cases clearly show two maxima at 70 and 158 K, respectively, indicative of a two-phase magnetization alignment process. The LS analyses can explain the shift of the ZFC magnetization maximum to lower temperatures in the BNSL membranes (158 K) versus the larger $Fe_3O_4$ NCs (209 K) as a mathematical superposition effect but is unable to account for the disappearance of the low-temperature peak associated with the smaller $Fe_3O_4$ NCs.

In BNSLs, the spacing between two neighboring NCs is ~2 nm, as each NC is capped by a layer of long-chain organic ligands (oleic acid).[34] Hence, the origin of the interaction effect observed in Figure 2 is more likely due to dipolar interactions[5] rather than exchange couplings,[19] which are comparatively negligible. Moreover, the BNSL structure is expected to maximize interactions between the two NC components when compared to random or phase-separated mixtures. The dipole−dipole interaction energy between two NCs can be expressed as[36]

$$E = \frac{\vec{\mu}_i \cdot \vec{\mu}_j}{r_{ij}^3} - \frac{3(\vec{\mu}_i \cdot \vec{r}_{ij})(\vec{\mu}_j \cdot \vec{r}_{ij})}{r_{ij}^5} \quad (2)$$

where $\vec{\mu}_i$ and $\vec{\mu}_j$ are magnetic moments of neighboring NCs $i$ and $j$, respectively, $\vec{r}_{ij}$ is a vector connecting the magnetic moments $i$ and $j$, and $r_{ij} = |\vec{r}_{ij}|$. We propose that dipole−dipole interactions between two NC components (A−B interactions) in BNSLs induce an additional energy barrier and the magnetic moments of the smaller B-site $Fe_3O_4$ NCs are pinned by the local dipolar field induced by the random magnetic moments of the larger A-site $Fe_3O_4$ NCs.[37,38] Thus, well below the blocking temperature of the A sublattice, the magnetic alignment of the B sublattice is suppressed as temperature increases. This manifests in the ZFC curves (Figure 2b) as the slower rise of the initial total magnetization in comparison with the phase-separated mixtures (regime I) and the disappearance of the low-temperature alignment peak (regime II). Because of the continuing moment alignment of the larger $Fe_3O_4$ NCs with the increasing temperature, the total magnetization further increases before reaching a maximum at 158 K. Increasing the temperature further provides enough thermal energy to overcome the dipolar interactions between two NC components,[35] such that the ZFC curve of the BNSL membrane essentially converges with that of the phase-separated mixtures (Figure 2b, regime III). In addition, the different curvature of the FC magnetization curves between BNSLs and the phase-separated mixtures also provides evidence of interparticle A−B interactions present in BNSLs. In the phase-separated NC mixture, the initial FC magnetization drops abruptly as temperature increases (Figure 2b, regimes I and II), corresponding to the



DOI: 10.1021/nl103568q | *Nano Lett.* **2010,** *10,* 5103–5108

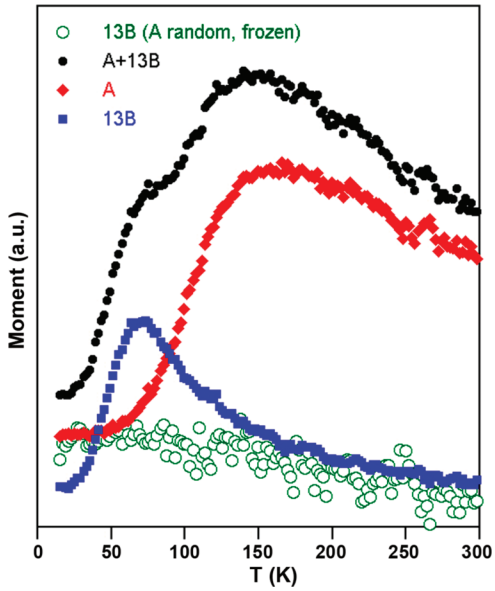


**FIGURE 3. Monte Carlo simulations of stoichiometrically weighted ZFC curves for 14.3 nm $Fe_3O_4$ NCs (red) and 7.2 nm $Fe_3O_4$ NCs (blue) in the dilute limit, and their sum (black). Also shown is the B sublattice response in the interacting $AB_{13}$ unit cell (olive) with the larger magnetic moment of A sites randomly frozen as discussed in the text.**

fast moment fluctuation of the smaller $Fe_3O_4$ NCs. By contrast, the thermally activated moment fluctuation of the smaller NCs is significantly suppressed in BNSLs, as evidenced by the diminished decrease rate of the initial FC magnetization. This is consistent with the pinning of the moment of the smaller $Fe_3O_4$ NCs by the random dipolar field exerted by the larger $Fe_3O_4$ NCs.

To explore this intuition, we have calculated the random dipolar fields and performed Monte Carlo simulation of ZFC curves in the $AB_{13}$ structure.[36,39] We find that for the ico-$AB_{13}$ structure with 14.3 and 7.2 nm $Fe_3O_4$ NCs the random internal magnetic field on the B sublattice has an average magnitude of 650 Oe with a standard deviation of 270 Oe. The internal magnetic field is therefore much stronger than the applied magnetic field of 100 Oe, and also significantly greater than the random magnetic field due to the B−B interactions alone (320 Oe with a standard deviation of 140 Oe). Thus, A−B interactions dominate the magnetic field environment for the B sublattice in the $AB_{13}$ superlattice structure. Our simulations employ measured magnetic moments and tuned anisotropies (see Methods in Supporting Information), and find generally good agreement with the ZFC data for individual dilute A and B NC components, as well as their weighted sum (Figure 3). We further demonstrate the effect of A−B interactions on the warming curve of the B sublattice within the $AB_{13}$ structure by freezing the A sublattice in random arrangements. The calculated B-sublattice ZFC curve is notably suppressed up to 300 K (Figure 3, olive curve), indicating that the random field due to the A sublattice largely blocks reorientation of the B sublattice. These numerical simulations therefore corroborate our intuitive arguments linking the disappearance of the B-related peak in the experimental ZFC curve of BNSLs.

It is interesting to note the BNSL membrane shows a similar low-temperature (15 K) magnetic hysteresis loop as the phase-separated NC mixture with coercivity located between that of the two NC components (Supporting Information Figure S6). However, the two $Fe_3O_4$ NC components are both soft magnets with close coercivities, 120 and 520 Oe, respectively, and have randomly oriented anisotropy axes that produce net hysteresis loops with broad reversals rather than square profiles. As a result, the hysteresis data do not clearly distinguish whether the BNSL displays a single- or two-phase magnetization reversal behavior. It is worth mentioning that if the two NC components possess dramatically different coercivities,[19] hysteresis loops should more easily test the coupling effects. In addition to phase-separated NC mixtures, we also compare the ZFC curve of BNSLs with that of a random NC mixture without long-range NC ordering (Supporting Information Figure S7). Although the random NC mixture also exhibits a magnetization alignment process (Supporting Information Figure S7b), the ZFC peak is significantly broader than that of BNSLs. We attribute this to the wider distribution of dipole−dipole interaction energy resulted from the nonuniform interparticle spacing in the random mixture, consistent with previous results on single-component NC assemblies.[5]

Similar collective dipolar coupling interactions are also observed in BNSLs having different structures (or stoichiometry). By adjusting the NC number ratio between two $Fe_3O_4$ NC components, we are able to tune the structure of BNSL membranes from ico-$AB_{13}$ to $AlB_2$ (Figure 4a), in which one layer of hexagonally packed larger NCs alternate with another layer of hexagonally packed smaller NCs. TEM reveals that these $AlB_2$-type BNSL membranes are consisting of a mosaic of binary superlattice domains with different growth directions and/or different lattice projections (Supporting Information Figure S8). Similar to ico-$AB_{13}$-type BNSL membranes, $AlB_2$-type BNSL membranes also show one maximum (178 K) in the ZFC curve and the low-temperature peak corresponding to the smaller $Fe_3O_4$ NCs disappears (Figure 4b, blue curve). We note that in the $AlB_2$-type BNSL structure, each individual smaller NC has six larger NC neighbors, such that the pinning effect of the larger $Fe_3O_4$ NCs on the smaller NCs through the dipolar field is expected to be even stronger than that in the ico-$AB_{13}$-type BNSL structure.

In addition to $Fe_3O_4$−$Fe_3O_4$ combinations, we also study the magnetic properties of BNSLs self-assembled from other NC combinations. Co-assembly of 14.3 nm $Fe_3O_4$ NCs and 6.0 nm FePt NCs results in large-area $AlB_2$-type BNSL membranes (Figure 5a), which also exhibit a single-phase-like magnetization alignment process in the ZFC curve (Figure 5b, blue curve), as revealed by the disappearance of the low-temperature peak corresponding to FePt NCs. In comparison, in the ZFC curve of the phase-separated NC mixture



DOI: 10.1021/nl103568q | *Nano Lett.* **2010,** *10,* 5103–5108

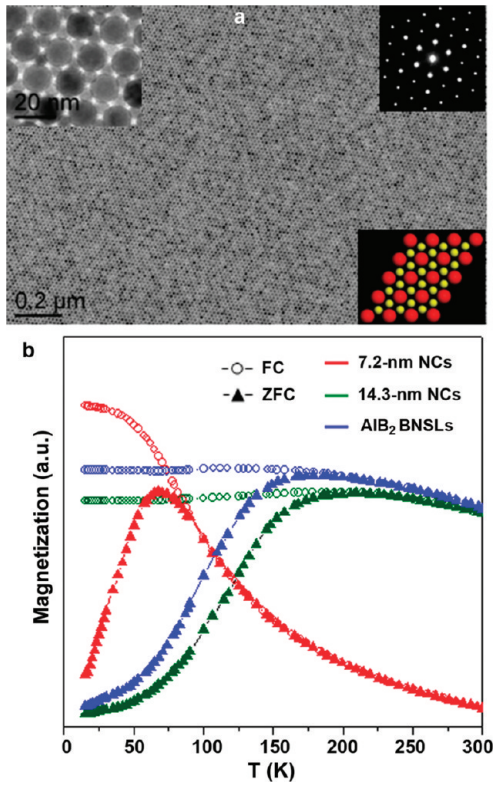


FIGURE 4. (a) TEM image, magnified view (upper left inset), small-angle electron diffraction pattern (upper right inset), and structural model (lower right inset) of a typical $AlB_2$-type BNSL membrane self-assembled from 14.3 and 7.2 nm $Fe_3O_4$ NCs along the (001) lattice projection. (b) ZFC/FC curves for 14.3 nm $Fe_3O_4$ NCs (olive), 7.2 nm $Fe_3O_4$ NCs (red), and the resulting $AlB_2$-type BNSL membrane (blue).

having the same $AB_2$ stoichiometry, two peaks corresponding to 14.3 nm $Fe_3O_4$ NCs and 6.0 nm FePt NCs are identified (Figure 5b, magenta curve). As in the case of the ico-$AB_{13}$-type $Fe_3O_4$—$Fe_3O_4$ BNSLs, the curvature difference of the FC magnetization between the $AlB_2$-type $Fe_3O_4$—FePt BNSL membrane and the phase-separated NC mixture in the low-temperature regime also demonstrates dipolar interparticle interactions present in BNSLs. To further understand the dipolar coupling effect, we intentionally prepare samples consisting of both $AlB_2$-type $Fe_3O_4$—FePt BNSLs and FePt single NC superlattices (area coverage, ~25%) by increasing the FePt/$Fe_3O_4$ NC number ratio (Figures 5c and Supporting Information S9). Under this situation, a low-temperature peak arising from FePt NC superlattices appears in the ZFC curve (Figure 5d), suggesting the magnetic moment of the excess FePt NCs can not be completely pinned by the dipolar field of $Fe_3O_4$ NCs. This also indicates that the ZFC magnetization measurement is sensitive to the "purity" of BNSLs.

In this work, we have studied interparticle dipole—dipole interactions in high-quality magnetic BNSL membranes grown by the liquid—air interfacial assembly approach. A single-phase-like magnetization alignment process, which is attributed to collective dipolar interactions between two NC components, is observed in several types of BNSLs having different structures and/or different NC combinations. Our experiments together with Monte Carlo simulation demonstrate the pinning effect that the larger NC sublattice has on the smaller NC sublattice through the dipolar field, which

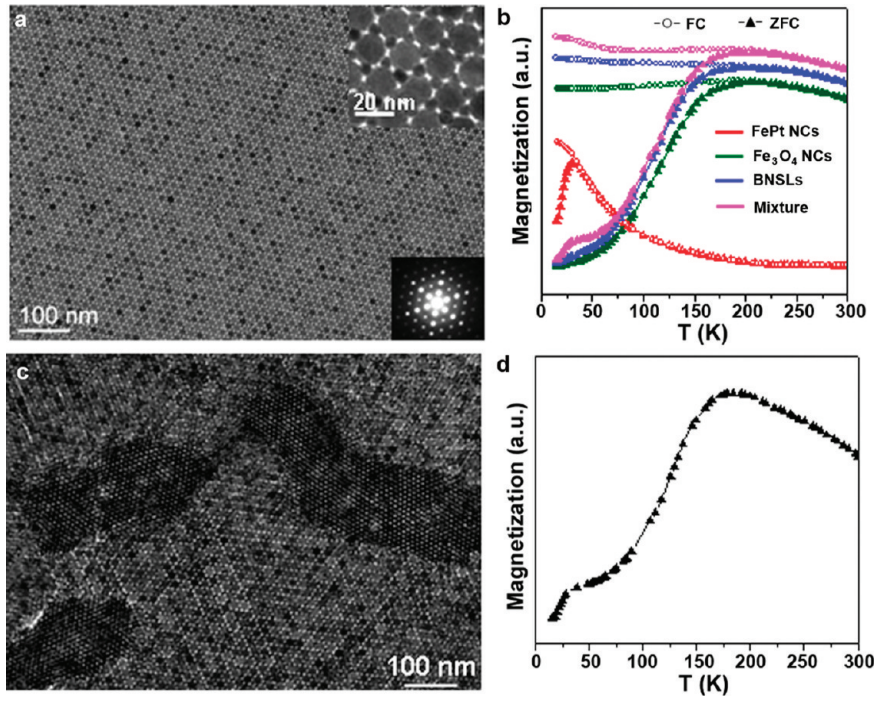


FIGURE 5. (a) TEM image, magnified view (upper right inset), and small-angle electron diffraction pattern (lower right inset) of a typical $AlB_2$-type BNSL membrane self-assembled from 14.3 nm $Fe_3O_4$ NCs and 6.0 nm FePt NCs along the (001) lattice projection. (b) ZFC/FC curves for 14.3 nm $Fe_3O_4$ NCs (olive), 6.0 nm FePt NCs (red), the resulting $AlB_2$-type BNSL membrane (blue), and a phase-separated NC mixture (magenta), respectively. (c) TEM image and (d) ZFC curve of an $AlB_2$-type $Fe_3O_4$—FePt BNSL membrane containing excess FePt NCs.



DOI: 10.1021/nl103568q | *Nano Lett.* **2010,** *10,* 5103–5108

accounts for the single-phase-like behavior observed in BNSLs. To the best of our knowledge, this is the first experimental demonstration of collective magnetic behaviors in multicomponent NC superlattices. The ability to probe interparticle interactions present in BNSLs is critical to designing novel NC-based metamaterials with rationally modulated properties.

**Acknowledgment.** J.Chen, A.D., and C.B.M. acknowledge the financial support from the U.S. Army Research Office (ARO) under award number MURI W911NF-08-1-0364 for nanocrystal synthesis, assembly and characterization. J.Cai and J.M.K. acknowledge the support from the NSF MRSEC program under award number DMR-0520020 for magnetometry and Monte Carlo simulations. X.Y. acknowledges support from the Department of Energy Basic Energy Science division under award number DE-SC0002158 for structural characterization. Y.J.K. acknowledges financial support from the U.S. Army Research Office (ARO) under award MURI W911NF-08-1-0364 for ICP measurement. A.D. also thanks the Molecular Foundry at Lawrence Berkeley National Lab for partial support. C.B.M. also thanks the Richard Perry University Professorship for partial support of his supervisor role. We thank Lolita Rotkina at the Penn Regional Nanotechnology Facility for support in SEM, and David Vann at Department of Earth and Environmental Science (University of Pennsylvania) for support in ICP-OES.

**Supporting Information Available.** Methods (synthesis and purification of NCs, self-assembly and transfer of BNSL membranes, instrumentation, and Monte Carlo simulations), size distribution of $Fe_3O_4$ NCs, magnetic hysteresis loops, ZFC measurements of a random NC mixture, and additional TEM and SEM images. This material is available free of charge via the Internet at http://pubs.acs.org.

## REFERENCES AND NOTES

(1) Sun, S.; Murray, C. B.; Weller, D.; Folks, L.; Moser, A. *Science* **2000**, *287*, 1989–1992.
(2) Talapin, D. V.; Murray, C. B. *Science* **2005**, *310*, 86–89.
(3) Collier, C. P.; Saykally, R. J.; Shiang, J. J.; Henrichs, S. E.; Heath, J. R. *Science* **1997**, *277*, 1978–1981.
(4) Tao, A. R.; Sinsermsuksakul, P.; Yang, P. *Nat. Nanotechnol.* **2007**, *2*, 435–440.
(5) Pileni, M. P. *Acc. Chem. Res.* **2007**, *40*, 685–693.
(6) Chen, M.; Nikles, D. E. *Nano Lett.* **2002**, *2*, 211–214.
(7) Bodnarchuk, M. I.; Kovalenko, M. V.; Pichler, S.; Fritz-Popovski, G.; Hesser, G.; Heiss, W. *ACS Nano* **2010**, *4*, 423–431.
(8) Redl, F. X.; Cho, K. S.; Murray, C. B.; O'Brien, S. *Nature* **2003**, *423*, 968–971.
(9) Shevchenko, E. V.; Talapin, D. V.; Kotov, N. A.; O'Brien, S.; Murray, C. B. *Nature* **2006**, *439*, 55–59.
(10) Dong, A.; Chen, J.; Vora, P. M.; Kikkawa, J. M.; Murray, C. B. *Nature* **2010**, *466*, 474–477.
(11) Cheon, J.; Park, J. I.; Choi, J. S.; Jun, Y. W.; Kim, S.; Kim, M. G.; Kim, Y. M.; Kim, Y. J. *Proc. Natl. Acad. Sci. U.S.A.* **2006**, *103*, 3023–3027.
(12) Chen, Z.; O'Brien, S. *ACS Nano* **2008**, *2*, 1219–1229.
(13) Smith, D. K.; Goodfellow, B.; Smilgies, D. M.; Korgel, B. A. *J. Am. Chem. Soc.* **2009**, *131*, 3281–3290.
(14) Friedrich, H.; Gommes, C. J.; Overgaag, K.; Meeldijk, J. D.; Evers, W. H.; de Nijs, B.; Boneschanscher, M. P.; de Jongh, P. E.; Verkleij, A. J.; de Jong, K. P.; van Blaaderen, A.; Vanmaekelbergh, D. *Nano Lett.* **2009**, *9*, 2719–2724.
(15) Sra, A. K.; Ewers, T. D.; Xu, Q.; Zandbergen, H.; Schaak, R. E. *Chem. Commun.* **2006**, 750–752.
(16) Chen, J.; Ye, X.; Murray, C. B. *ACS Nano* **2010**, *4*, 2374–2381.
(17) Urban, J. J.; Talapin, D. V.; Shevchenko, E. V.; Kagan, C. R.; Murray, C. B. *Nat. Mater.* **2007**, *6*, 115–121.
(18) Shevchenko, E. V.; Ringler, M.; Schwemer, A.; Talapin, D. V.; Klar, T. A.; Rogach, A. L.; Feldmann, J.; Alivisatos, A. P. *J. Am. Chem. Soc.* **2008**, *130*, 3274–3275.
(19) Zeng, H.; Li, J.; Liu, J. P.; Wang, Z. L.; Sun, S. *Nature* **2002**, *420*, 395–398.
(20) Zeng, H.; Li, J.; Wang, Z. L.; Liu, J. P.; Sun, S. H. *Nano Lett.* **2004**, *4*, 187–190.
(21) Kang, S. S.; Miao, G. X.; Shi, S.; Jia, Z.; Nikles, D. E.; Harrell, J. W. *J. Am. Chem. Soc.* **2006**, *128*, 1042–1043.
(22) Bodnarchuk, M. I.; Kovalenko, M. V.; Groiss, H.; Resel, R.; Reissner, M.; Hesser, G.; Lechner, R. T.; Steiner, W.; Schaffler, F.; Heiss, W. *Small* **2009**, *5*, 2247–2252.
(23) Russier, V.; Petit, C.; Legrand, J.; Pileni, M. P. *Phys. Rev. B* **2000**, *62*, 3910–3916.
(24) Fried, T.; Shemer, G.; Markovich, G. *Adv. Mater.* **2001**, *13*, 1158–1161.
(25) Puntes, V. F.; Krishnan, K. M.; Alivisatos, P. *App. Phys. Lett.* **2001**, *78*, 2187–2189.
(26) Song, Q.; Zhang, Z. J. *J. Am. Chem. Soc.* **2004**, *126*, 6164–6168.
(27) Puntes, V. F.; Gorostiza, P.; Aruguete, D. M.; Bastus, N. G.; Alivisatos, A. P. *Nat. Mater.* **2004**, *3*, 263–268.
(28) Vestal, C. R.; Song, Q.; Zhang, Z. J. *J. Phys. Chem. B* **2004**, *108*, 18222–18227.
(29) Luo, W.; Nagel, S. R.; Rosenbaum, T. F.; Rosensweig, R. E. *Phys. Rev. Lett.* **1991**, *67*, 2721–2724.
(30) Bae, C. J.; Angappane, S.; Park, J. G.; Lee, Y.; Lee, J.; An, K.; Hyeon, T. *Appl. Phys. Lett.* **2007**, *91*, 102502.
(31) Poddar, P.; Telem-Shafir, T.; Fried, T.; Markovich, G. *Phys. Rev. B* **2002**, *66*, No. 060403.
(32) Georgescu, M.; Klokkenburg, M.; Erne, B. H.; Liljeroth, P.; Vanmaekelbergh, D.; van Emmichoven, P. A. Z. *Phys. Rev. B* **2006**, *73*, 184415.
(33) Georgescu, M.; Viota, J. L.; Klokkenburg, M.; Erne, B. H.; Vanmaekelbergh, D.; van Emmichoven, P. A. Z. *Phys. Rev. B* **2008**, *77*, No. 024423.
(34) Park, J.; An, K. J.; Hwang, Y. S.; Park, J. G.; Noh, H. J.; Kim, J. Y.; Park, J. H.; Hwang, N. M.; Hyeon, T. *Nat. Mater.* **2004**, *3*, 891–895.
(35) Trudel, S.; Hill, R. H. *Polyhedron* **2007**, *26*, 1863–1870.
(36) Garcia-Otero, J.; Porto, M.; Rivas, J.; Bunde, A. *Phys. Rev. Lett.* **2000**, *84*, 167–170.
(37) Trudel, S.; Hill, R. H. *J. Magn. Magn. Mater.* **2007**, *310*, 2516–2517.
(38) Vargas, J. M.; Nunes, W. C.; Socolovsky, L. M.; Knobel, M.; Zanchet, D. *Phys. Rev. B* **2005**, *72*, 184428.
(39) Kechrakos, D.; Trohidou, K. N. *Appl. Phys. Lett.* **2002**, *81*, 4574–4576.



DOI: 10.1021/nl103568q | *Nano Lett.* **2010,** *10,* 5103–5108